Toxicology and Applied Pharmacology 350 (2018) 52–63

Contents lists available at ScienceDirect

Toxicology and Applied Pharmacology

journal homepage: www.elsevier.com/locate/taap

Feraheme® suppresses immune function of human T lymphocytes through mitochondrial damage and mitoROS production

Ankit Shah[a], Cassandra I. Mankus[a], Alison M. Vermilya[a], Ferri Soheilian[b], Jeffrey D. Clogston[a], Marina A. Dobrovolskaia[a,*]

[a] Nanotechnology Characterization Laboratory, Cancer Research Technology Program, Leidos Biomedical Research, Inc., Frederick National Laboratory for Cancer Research, Frederick, MD 21702, USA
[b] Electron Microscopy Laboratory, Leidos Biomedical Research, Inc, Frederick National Laboratory for Cancer Research, Frederick, MD 21702, USA

ARTICLE INFO

Keywords:
Iron oxide
Nanoparticles
T Cells
Immunotoxicity
Immunosuppression

ABSTRACT

Despite attractive properties for both therapeutic and diagnostic applications, the clinical use of iron oxide nanoparticles (IONPs) is limited to iron replacement in severely anemic patient populations. While several studies have reported about the immunotoxicity of IONPs, the mechanisms of this toxicity are mostly unknown. We conducted a mechanistic investigation using an injectable form of IONP, Feraheme®. In the cultures of primary human T cells, Feraheme induced miotochondrial oxidative stress and resulted in changes in mitochondrial dynamics, architecture, and membrane potential. These molecular events were responsible for the decrease in cytokine production and proliferation of mitogen-activated T cells. The induction of mitoROS by T cells in response to Feraheme was insufficient to induce total redox imbalance at the cellular level. Consequently, we resolved this toxicity by the addition of the mitochondria-specific antioxidant MitoTEMPO. We further used these findings to develop an experimental framework consisting of critical assays that can be used to estimate IONP immunotoxicity. We explored this framework using several immortalized T-cell lines and found that none of them recapitulate the toxicity observed in the primary cells. Next, we compared the immunotoxicity of Feraheme to that of other FDA-approved iron-containing complex drug formulations and found that the mitochondrial damage and the resulting suppression of T-cell function are specific to Feraheme. The framework, therefore, can be used for comparing the immunotoxicity of Feraheme with that of its generic versions, while other iron-based complex drugs require case-specific mechanistic investigation.

1. Introduction

A variety of iron oxide nanoparticles (IONPs) is explored for both diagnostic and therapeutic applications due to their superparamagnetic properties (Li et al., 2017; Nedyalkova et al., 2017). Some IONPs intended for use as magnetic resonance imaging contrast agents have failed in clinical settings, and immune-mediated toxicities, such as hypersensitivity reactions, contributed to the reasons for their withdrawal from the market (Wysowski et al., 2010; Valdiglesias et al., 2016). Some of these reactions are believed to be pseudoallergies, which occur due to the nanoparticle binding to and activating the complement proteins (Hempel et al., 2017).

Nanoparticle coating is thought to be the primary structural component that contributes to the complement-mediated immunotoxicity. Notably, iron dextran and ferric carboxymaltose activate the complement system, while ferumoxytol and iron isomaltoside do not (Hempel et al., 2017). Interestingly, iron sucrose complexes bind to the complement without activating it (Hempel et al., 2017). The role of the iron core in the complement activation is unknown.

The majority of published studies attribute the cell-mediated immunotoxicity of IONPs to the mononuclear phagocytic system, which plays a central role in nanoparticle clearance from systemic circulation (Di Gioacchino et al., 2011; Pouliquen et al., 1991; Sadauskas et al., 2009; Umbreit et al., 2012). Indeed, several studies have shown an increase in oxidative stress and cytokines in the macrophages upon treatment with IONPs, both in vitro and in vivo (Lunov et al., 2010; Naqvi et al., 2010; Sabareeswaran et al., 2016; Pai et al., 2011). Similarly, mitochondrial damage and endoplasmic reticulum stress were shown to be responsible for the apoptosis in macrophages and lymphocytes exposed to the IONPs (Park et al., 2014; Gaharwar et al., 2017). Immunomodulation and elevation of proinflammatory cytokines in response to IONPs were reported in a T-cell line in vitro (Yan et al., 2015). Similarly, the pulmonary accumulation of IONPs in an in vivo mouse model resulted in Th1 immune response (Park et al., 2015). Like

* Corresponding author at: Leidos Biomedical Research, Inc., P.O. Box B, 1050 Boyles Street, Frederick, MD 21702–1201, USA.
E-mail address: marina@mail.nih.gov (M.A. Dobrovolskaia).

https://doi.org/10.1016/j.taap.2018.04.028
Received 6 January 2018; Received in revised form 19 April 2018; Accepted 20 April 2018
Available online 30 April 2018
0041-008X/

the complement-mediated pseudoallergic reactions, the cell-mediated toxicity of IONPs is also attributed to the iron coating (Valdiglesias et al., 2016; Turcheniuk et al., 2013). In contrast to the studies demonstrating IONPs' ability to stimulate an immune response, a few recent reports have shown that IONPs could also be immunosuppressive, as evidenced by a decrease in the ovalbumin (OVA)-specific antibodies in mice following animal exposure to these particles (Shen et al., 2011a).

Cellular and molecular mechanisms, which could shed light on the differences between immunostimulatory and immunosuppressive IONPs, are poorly understood. Nevertheless, the available data regarding IONPs' ability both to activate a T cell–mediated immune response (Yan et al., 2015; Park et al., 2015) and to suppress delayed-type hypersensitivity (DTH) reactions (20) and OVA-specific antibody production (Shen et al., 2011a) point toward IONP interactions with T cells, which serve as a common key contributor to both types of these toxicities.

To cover the current gap in the understanding of IONP interactions with T cells, we conducted an in vitro study using an injectable form of IONP, Feraheme®. We chose this formulation because it is approved for clinical use in the U.S., and its analog European formulation, Resovist, was used in the studies that reported suppression of DTH and formation of antibodies to OVA (Shen et al., 2011a, 2012, 2011b). We investigated cellular and molecular changes in primary human T lymphocytes following Feraheme treatment. The goal of the study was to understand the molecular mechanism underlying Feraheme-mediated effects on T-cells, verify the association of this mechanism with the changes in T-cell function, and use this information to compile a framework of in vitro assays that could be used to screen generic versions of Feraheme for potential differences from the reference listed drug. We also wanted to understand whether other iron-based complex drug formulations share Feraheme's molecular pathways and immunotoxicity, as well as whether the compiled assay network selected in the study of Feraheme can be broadly applied to other iron-based formulations. Lastly, we wanted to understand whether primary human T lymphocytes can be substituted with any of the currently available immortalized T-cell lines.

2. Materials and methods

2.1. Reagents

All the experiments were performed using primary T cells obtained from the human blood collected under the research donor program at the National Cancer Institute (NCI) at Frederick, described below. Feraheme (AMAG Pharmaceuticals, Waltham, MA); Venofer® and Injectafer® (American Regent, Inc., Shirley, NY); Ferrlecit® (Sanofi-Aventis U.S. LLC, Bridgewater, NJ); and a generic version of Ferrlecit, sodium ferric gluconate (West-Ward Pharma, Eatontown, NJ), were purchased from the National Institutes of Health pharmacy. The specific inhibitors Deferoxamine mesylate salt, Cytochalasin D, MitoTEMPO, chlorpromazine, and Filipin III were obtained from Sigma-Aldrich (St. Louis, MO). The reactive oxygen species (ROS) detection probes CM-H_2DCFDA and CellROX™ green were obtained from Life Technologies, Inc. (Carlsbad, CA). MitoSOX™ was obtained from Molecular Probes, Inc. (Eugene, OR). The antibodies used for different applications were obtained from various sources as listed in Supplementary Table 1. The cell proliferation BrdU kit was from Millipore (EMD Millipore, Billerica, MA). Vacutainer tubes were from BD (Franklin Lakes, NJ). Glutamine, fetal bovine serum (FBS), and penicillin/streptomycin were from HyClone (Logan, UT). RPMI-1640 was from Invitrogen/Life Technologies (Carlsbad, CA). Ficoll-Paque™ Premium was from GE Healthcare (Piscataway, NJ).

2.2. Cell lines

Mo-T, Loucy, and A3 leukemia cell lines were purchased from ATCC (Manassas, VA).

2.3. Research donor blood

Healthy volunteer blood was collected under NCI at Frederick Protocol OH99-C-N046. Blood was drawn into BD vacutainer tubes containing Li-heparin as the anticoagulant, then kept at room temperature and used within two hours after collection.

2.4. Isolation of primary human T cells

Primary T cells were isolated from the heparinized blood of healthy donors by using the RosetteSep™ Human T Cell Enrichment Cocktail from STEMCELL Technologies, Inc., (Cambridge, MA) according to the manufacturer's protocol. Briefly, heparinized blood was incubated with 1 mL of RosetteSep for every 20 mL of blood at room temperature (RT) for 20 min. Following incubation, the blood was mixed with an equal volume of phosphate-buffered saline (PBS) supplemented with 2% FBS and overlaid on Ficoll-Paque Premium. The tubes were centrifuged at RT and 1200*g* for 20 min with minimum acceleration and break, the interphase containing the cell layer was collected and washed twice with PBS, and the cells were resuspended in complete medium (RPMI-1640, 10% FBS, 2 mM L-glutamine, 100 U/mL penicillin, and 100 μg/mL streptomycin sulfate). The cell viability, cell count, and phenotyping were assessed to verify the quality and purity of T cells. All of the experiments, unless specified otherwise, were performed in 48-well plates with 400×10^3 cells in 500 μL of complete medium per well.

2.5. Mitochondrial reactive oxygen species (mitoROS) measurement

Unless specified otherwise, primary T cells were incubated with the treatment for 24 h before analysis of ROS levels. At the end of the incubation time, the cells were washed twice with PBS. Pelleted cells were then resuspended in 300 μL of MitoSOX Red (Molecular Probes, Inc., Eugene, OR) for mitoROS detection. The assay was performed according to the manufacturer's protocol, with H_2O_2 as a positive control to qualify the assay performance. Briefly, the cells were incubated with MitoSOX for 30 min, then washed with PBS to remove excess dye. The samples were immediately analyzed with the FL2 channel for mitoROS measurement using FACSCalibur and CellQuest software from BD Biosciences (San Jose, CA). The data were analyzed for relative changes in mitoROS intensities as compared to the negative control by using FCS Express 5.0 from De Novo Software (Glendale, CA). For the experiment involving the inhibitor MitoTEMPO, cells were pre-incubated with MitoTEMPO for 30 min before treatment with test samples.

2.6. Glutathione (GSH) assay

The assessment of oxidative stress was performed using the GSH-Glo™ Glutathione Assay from Promega Corporation (Madison, WI) following the manufacturer's protocol. Briefly, the primary T cells were isolated as described above, and 100,000 cells per well in a 96-well plate were incubated with different treatments for 24 h. Diethyl maleate was used as a positive control and added to the appropriate wells at 0.5 mM concentrations. After the treatment, the supernatants were removed and washed twice with PBS. The cells were then incubated with GSH-Glo™ Reagent for 30 min, which was followed by incubation with luciferin detection reagent for 15 min, after which the luminescence was measured using a SpectraMax M5 plate reader from Molecular Devices (Sunnyvale, CA). The GSH standard curve was used to calculate absolute GSH concentrations indicative of oxidative stress.

2.7. Loss of mitochondrial membrane potential (Δψm)

Loss of mitochondrial membrane potential was measured using the MitoProbe™ JC-1 Assay from Molecular Probes, Inc., (Eugene, OR) according to the manufacturer's protocol. Briefly, following treatment, the cells were washed twice with PBS, and the pellets were incubated with JC-1 dye solution for 15 min. After the incubation, the cells were washed once with PBS to deplete unbound dye, and samples were acquired on FACSCalibur with CellQuest software. FCCP was used as a positive control to gate the FL1 vs. FL2 plots, and the percentage of cells in FL1 was used as a measure of depolarized mitochondria. The Δψm was then calculated by normalizing the percentage of FL1-positive cells in treatment with that in the negative control. Gating strategy and representative fluorescent plots are shown in Supplementary Fig. 1.

2.8. Cytokine array analysis

The cytokine induction from T cells was assessed using a Q-Plex™ Array and custom multiplex assay plates (Quansys Biosciences, Logan, UT) per the manufacturer's recommended protocol. The experiment was performed according to the schematic shown in Fig. 5A. Briefly, 4×10^5 primary T cells from human blood were incubated with the test samples in 0.5 mL of culture medium for 24 h, which was followed by the addition of either 5 μg/mL OKT3 antibody or a cocktail containing 10 μg/mL PHA-M and 5 μg/mL ConA with or without test samples. The culture supernatants were collected at the termination of the experiment and stored at −80 °C until further use. The cytokines were captured on multiplex plates, and the images were acquired using Q-View Imager Pro™ with tandem analysis using Q-View software.

2.9. BrdU cell proliferation assay

The T-cell proliferation assay was performed using a BrdU Cell Proliferation Kit (EMD Millipore, Billerica, MA) per the manufacturer's protocol. The experiment was performed as described in Fig. 4B. After the treatment with test samples for 24 h, 5 μg/mL CD3-OKT3 was added, and the incubation continued with or without test samples for an additional 72 h. Finally, the BrdU reagent was added to the cells, and treatment was terminated after overnight (12–16 h) incubation. The BrdU incorporation was assessed using the horseradish peroxidase colorimetric activity method. SpectraMax M5 plate reader set at 450 and 540 nm, and SoftMax Pro software were used to measure optical density and analyze the data, respectively. The proliferation index was calculated by subtracting absorbance values in the non-BrdU control from that in the test samples, then normalizing the absorbance in the test samples with that in the negative control.

2.10. Western blotting

Western blotting for various signaling molecules was performed using whole-cell lysates from T cells. Briefly, T cells were exposed to the test samples for 24 h, and treatments were terminated by washing the cells with PBS. The cells were lysed with a radioimmunoprecipitation assay (RIPA) buffer (Boston BioProducts, Ashland, MA) containing Halt™ Protease and Phosphatase Inhibitor Cocktail (Thermo Fisher Scientific, Inc., Waltham, MA) for 10 min at 4 °C, which was followed by sonication for 10 s at one amplitude for complete lysis. Protein concentrations in the lysates were measured using a BCA protein assay kit (Thermo Fisher Scientific, Inc.), and 20 μg protein was separated on Novex 4–20% Tris-glycine gels, which was followed by transfer onto a polyvinylidene difluoride membrane. The blots were probed for appropriate targets using primary and secondary antibodies, and protein bands were visualized using Pierce ECL Plus reagent. The blot images were acquired using a G:BOX Chemi XX9 gel documentation system and GeneSys software from Syngene USA (Frederick, MD). All of the images were adjusted for brightness and contrast throughout the blots before undergoing band intensity quantification with ImageJ software. Relative changes in target proteins were calculated by normalizing the intensity of target proteins with β-actin as a loading control then comparing the treated samples with vehicle control.

2.11. Co-immunoprecipitation

The apoptosome formation in the T cells was assessed by analyzing pro-caspase-9 co-immunoprecipitates for the presence of cytochrome C and APAF1 using a kit for crosslink immunoprecipitation (IP) from Thermo Fisher Scientific, Inc. Briefly, after the treatment with the test material, the cells were lysed in the IP lysis buffer, and the equi-mass whole-cell lysate proteins were immobilized on an agarose-crosslinked antibody against pro-caspase-9. The antigen–antibody conjugates were washed to remove unbound proteins, the antigen complex was eluted with neutralizing pH buffer, and the eluates were separated on Tris-glycine gels followed by analysis by Western blotting. The immunoblots were then probed to detect the presence of cytochrome C and APAF1 in the pro-caspase-9 immunocomplex.

2.12. Prussian blue staining

Perls' Prussian blue reagent was used to detect iron uptake following different formulations. Briefly, 2×10^6 cells were treated with either test samples or vehicle control for 24 h in a six-well plate. After the treatment, the cells were washed twice with PBS to remove excess particles. Next, 200×10^3 cells were transferred onto glass slides using a cytospin centrifuge from Thermo Fisher Scientific, Inc., (Waltham, MA) at 1500 rpm for 10 min and fixed in 2% paraformaldehyde for 20 min at RT. The slides were washed and incubated with Perls' Prussian blue reagent (1:1 mixture of 2% potassium ferrocyanide in 2% hydrochloric acid) for 30 min at RT. Finally, the samples were stored with VECTASHIELD HardSet Antifade Mounting Medium (Vector Laboratories, Burlingame, CA), and the images were obtained at 1000 times magnification using a light microscope to visualize the presence of the purple-colored aggregates indicative of iron uptake.

2.13. Physicochemical characterization of IONPs

The IONP formulations used in the current study were analyzed using the dynamic light scattering, Zetasizer, and inductively coupled plasma mass spectrometry (ICP-MS) methods described in the Supplementary Methods section.

2.14. Statistical analysis

To perform statistical analysis, we used GraphPad Prism 7 software. The multiparametric comparisons were made with one-way ANOVA, and the differences were considered statistically significant with p-values ≤ 0.05 (*) or 0.01 (**).

3. Results

3.1. Feraheme alters mitochondrial architecture and dynamics in the primary human T cells

We isolated primary T cells from at least 10 healthy donors and analyzed the cells in vitro before and after Feraheme treatment using a JC-1 monomer formation assay. This test allowed us to understand IONP effects on the mitochondrial membrane potential. An increase in the JC-1 monomer formation is an indicator of the loss of Δψm (Perelman et al., 2012) (Supplementary Fig. 1). A 1.8 ± 0.2–fold increase in JC-1 monomers was detected in Feraheme-treated cells as compared to the negative controls (Fig. 1A). This response was concentration-dependent (Supplementary Fig. 2A–C) and donor-specific in that cells of 29% of the donors demonstrated maximum Δψm at a time

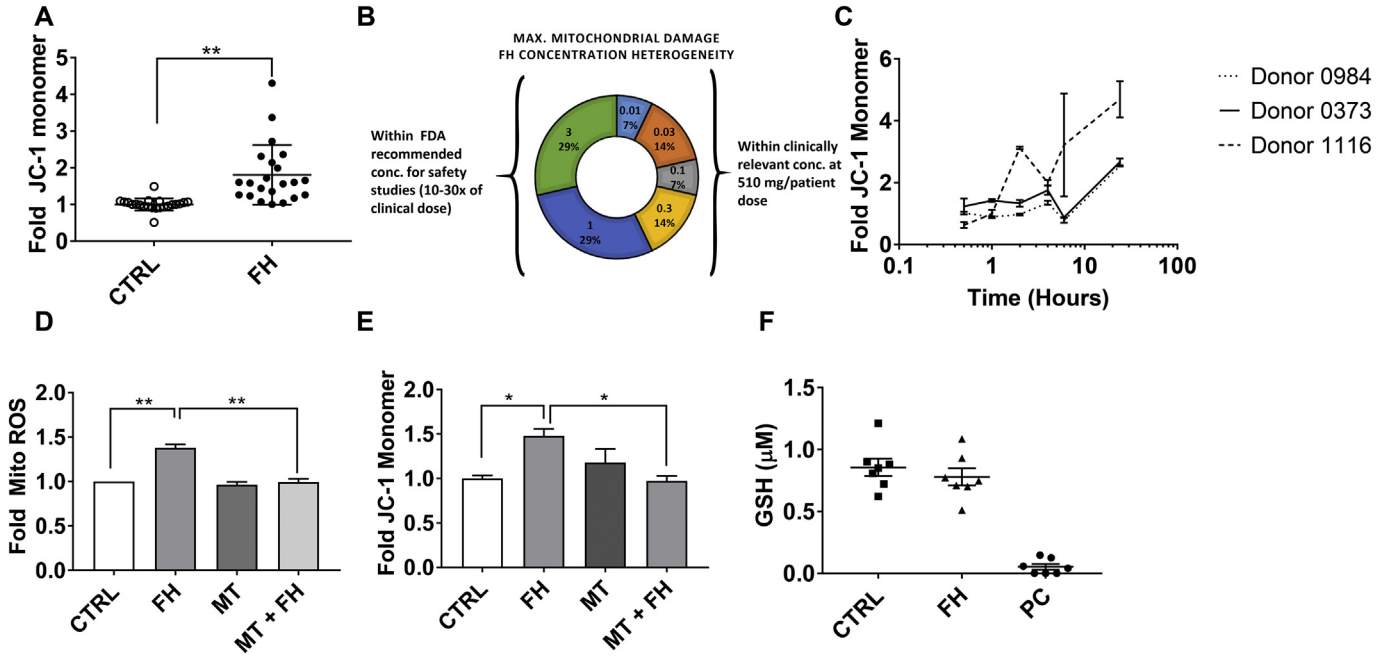

Fig. 1. Feraheme (FH) treatment induced mitochondrial damage in primary human T cells. Mitochondrial damage in response to varying concentrations of FH was assessed using a JC-1 assay in primary T cells obtained from at least 3 donors. (A) FH-treated T cells showed higher JC-1 monomers compared to the vehicle control, indicating mitochondrial membrane potential loss (Δψm) after 24 h. The data are presented as mean ± SEM (n = 11 donors) with experimental duplicates for each donor. (B) The T cells obtained from different donors demonstrated heterogeneity when assessed for the Δψm at different concentrations of FH for respective donors. The concentration of Feraheme that resulted in a maximum change in the Δψm at the 24-hour time point in a particular donor as the optimal concentration for that donor. It also has clinical relevance and may explain heterogeneity in the incidence of this toxicity among patients (C) Treatment with the optimum concentration of FH showed Δψm in respective donors in a time-dependent fashion. (D) FH-mediated mitochondrial oxidative stress was assessed using MitoSOX dye, which demonstrated an increase compared to vehicle-treated control. The increase in mitoROS was completely abolished with MitoTEMPO (MT). (E) Reducing mitoROS with MitoTEMPO also led to a reduction in FH-mediated Δψm. (F) The total oxidative stress, assessed using a GSH assay, remained unchanged in FH-treated cells compared to the vehicle control. The data are presented in mean ± SEM (n ≥ 3 donors) with experimental duplicates for each donor. * and ** denote p-value ≤.05 and ≤ 0.01, respectively. Each point on the line graph denotes mean ± SEM for the specific donor as identified in the plot with experimental duplicates for each time point.

point of 24 h and Feraheme concentrations of 3 mg/mL, while another 29% responded to 1 mg/mL, 14% to 0.3 mg/mL, 7% to 0.1 mg/mL, 14% to 0.03 mg/mL, and 7% to 0.01 mg/mL (Fig. 1B). We considered the concentration of Feraheme that resulted in a maximum change in the Δψm at the 24-hour time point in a particular donor as the optimal concentration for that donor. The response was also time-dependent, as evidenced by the JC-1 monomer accumulation in cells treated with the optimal concentration of Ferahame at different time points within the 24-hour time frame (Fig. 1C and Supplementary Fig. 2 D–F). Since the response was heterogeneous between individual donors and be consistent in all subsequent studies, we treated cells from individual donors using the optimal concentration specific to each donor.

Mitochondrial membrane potential is tightly associated with mitochondrial redox states (Kroemer et al., 2007). Therefore, we next measured the formation of mitoROS using the MitoSOX reagent (Fig. 1D). The Feraheme treatment increased mitoROS formation by 33 ± 4% (Fig. 1D). This increase was overcome when we performed the Ferahame treatment in the presence of the mitochondria-specific ROS inhibitor MitoTEMPO (Fig. 1D). Consistent with this result, MitoTEMPO also reduced the JC-1 accumulation in Feraheme-treated T cells (Fig. 1E). Next, we determined the levels of total oxidative stress using different ROS-sensing fluorescent reagents (Supplementary Fig. 3). Despite general recognition of the mitochondrial involvement in the generation of total ROS (Kroemer et al., 2007), we did not observe a significant increase in total ROS in the Feraheme-treated T cells. To further verify these data, we conducted a glutathione assay, which demonstrated no change in the levels of GSH after treatment with Feraheme (Fig. 1F).

Further assessment of the Feraheme-treated cells using transmission electron microscopy (TEM) revealed salient features of the mitochondrial damage (Fig. 2A). In particular, the mitochondrial cristae were collapsed in Feraheme-treated T cells as opposed to healthy mitochondria in the negative control. Moreover, remodeled cristae were observed more frequently in the Feraheme-treated cells (75.93%) as compared to the negative control (35.19%). Feraheme treatment also resulted in a gross alteration of mitochondrial dynamics, as evidenced by the presence of fused mitochondria (Fig. 2A–B). Feraheme-treated cells also demonstrated an increase in the number of mitochondria per cell (Fig. 2C), the phenomenon known as mitochondrial fission.

3.2. Feraheme activates apoptotic cascades without inducing cell death

The damaged mitochondria are known to trigger a cascade of events via cytochrome C release in the cytoplasm (Eleftheriadis et al., 2016; Ow et al., 2008). We, therefore, next assessed the signaling events following mitoROS generation and loss in Δψm. Treatment with Feraheme increased the levels of APAF1 in the T cells (Fig. 3A). Since cytochrome C and APAF1 interact with and recruit pro-caspase-9 to form the apoptosome (Ow et al., 2008), we co-immunoprecipitated pro-caspase-9, then conducted immunoblotting for cytochrome C and APAF1. An increase in the levels of APAF1 and cytochrome C in the pull-down fraction was detected in the Feraheme-treated cells (Fig. 3B). In agreement with these data, we also observed an increase in the cleaved products of caspase-9 and caspase-3 (Fig. 3C). The cell viability, however, was not affected (Supplementary Fig. 4).

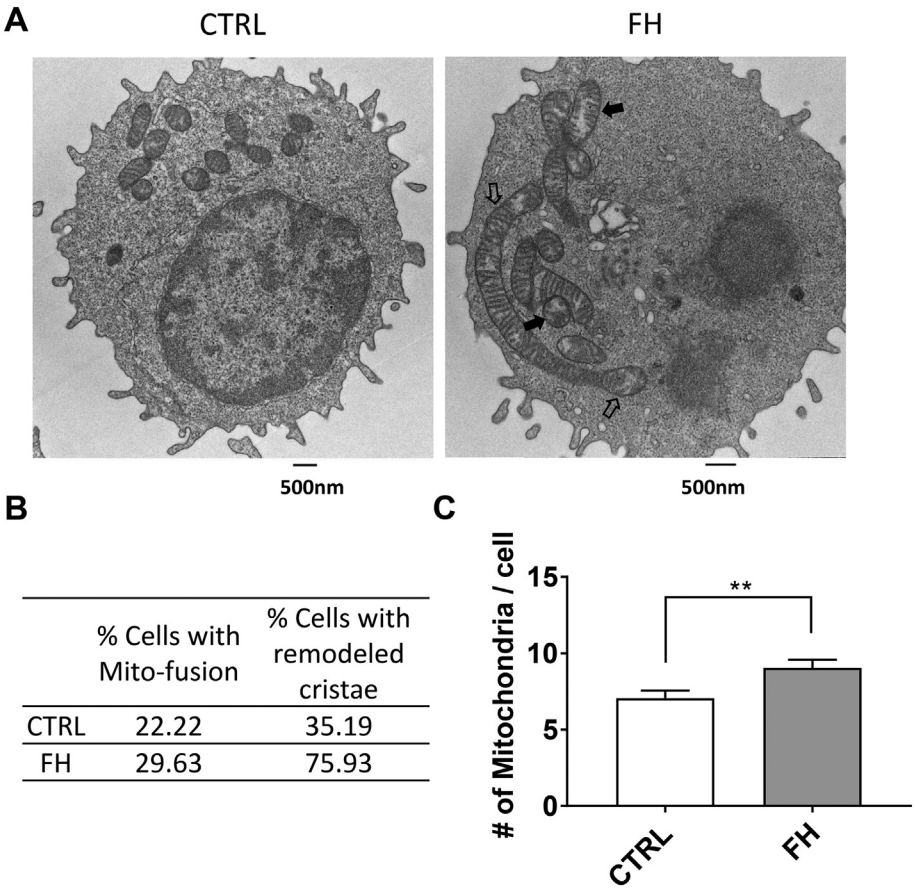

	% Cells with Mito-fusion	% Cells with remodeled cristae
CTRL	22.22	35.19
FH	29.63	75.93

Fig. 2. Feraheme (FH)-mediated mitochondrial damage and alteration of mitochondrial dynamics. (A) TEM images of T cells treated with FH show salient contrast compared to the vehicle control. Black arrows demonstrate mitochondria with remodeled cristae, and open arrows demonstrate fused mitochondria. (B) The percent of cells with mitochondrial fission and fusion was higher in FH-treated cells as opposed to the vehicle treatment. (C) The average number of mitochondria per cell was higher in the FH-treated group compared to that in the control. The quantification was performed with at least 75 random electron micrographs in each group. The bar graph is presented in mean ± SEM, and ** denotes p-value ≤ 0.01.

3.3. Feraheme influences intracellular iron homeostasis of the primary human T cells

To determine if the mitochondrial damage is associated with intracellular iron accumulation, we stained T cells with Prussian blue reagent. This reagent results in the formation of a blue colour after complexation with iron ions, and is commonly used to assess iron accumulation in cells and tissues. This staining revealed the formation of a blue punctae that preferentially located along the cell edge and polarized toward one side of the Feraheme-treated T cells (Fig. 4A).

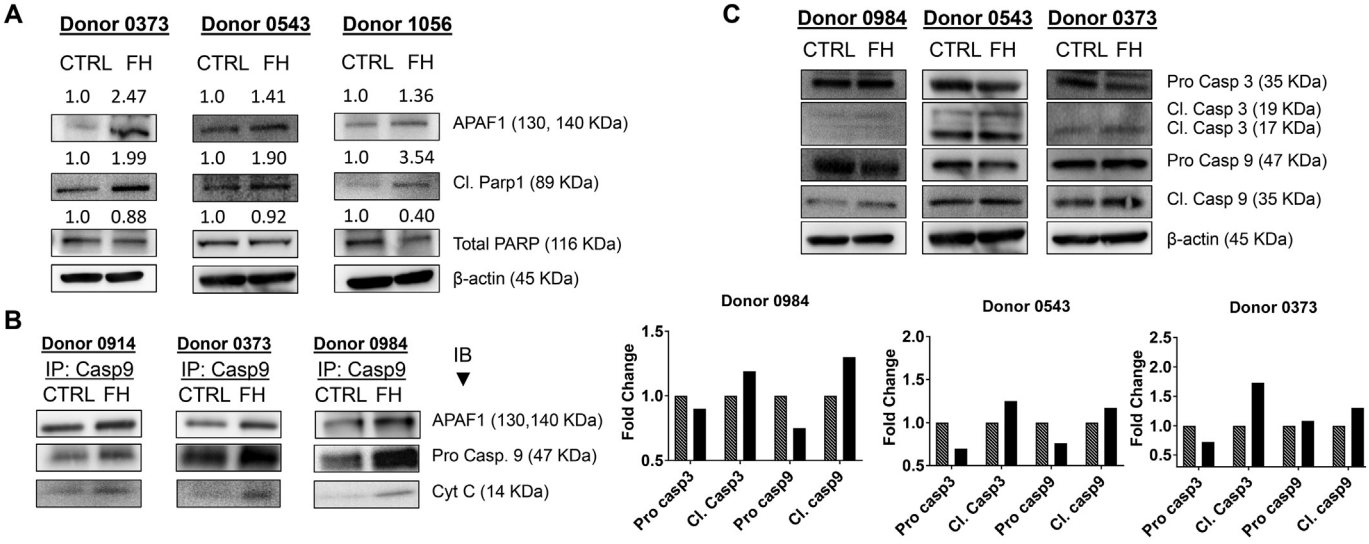

Fig. 3. Feraheme (FH) treatment activated apoptotic cascades in primary human T cells. Western blots show changes in downstream molecular events due to mitochondrial damage. (A) After 24 h of exposure, FH treatment increased the expression of APAF1 and triggered cleavage of PARP. (B) The co-immunoprecipitation for caspase-9 showed the presence of other apoptosome proteins in the FH-treated group, indicating activation of the downstream cascade. (C) The whole-cell lysates demonstrated an increase in cleaved caspase-3 and -9 due to FH treatment. The numbers above each blot represent the band intensity normalized with β-actin as loading control followed by negative control. Similarly, the bar graphs below the blots represent the band intensities for the respective donors, normalized with β-actin as loading control followed by negative control.

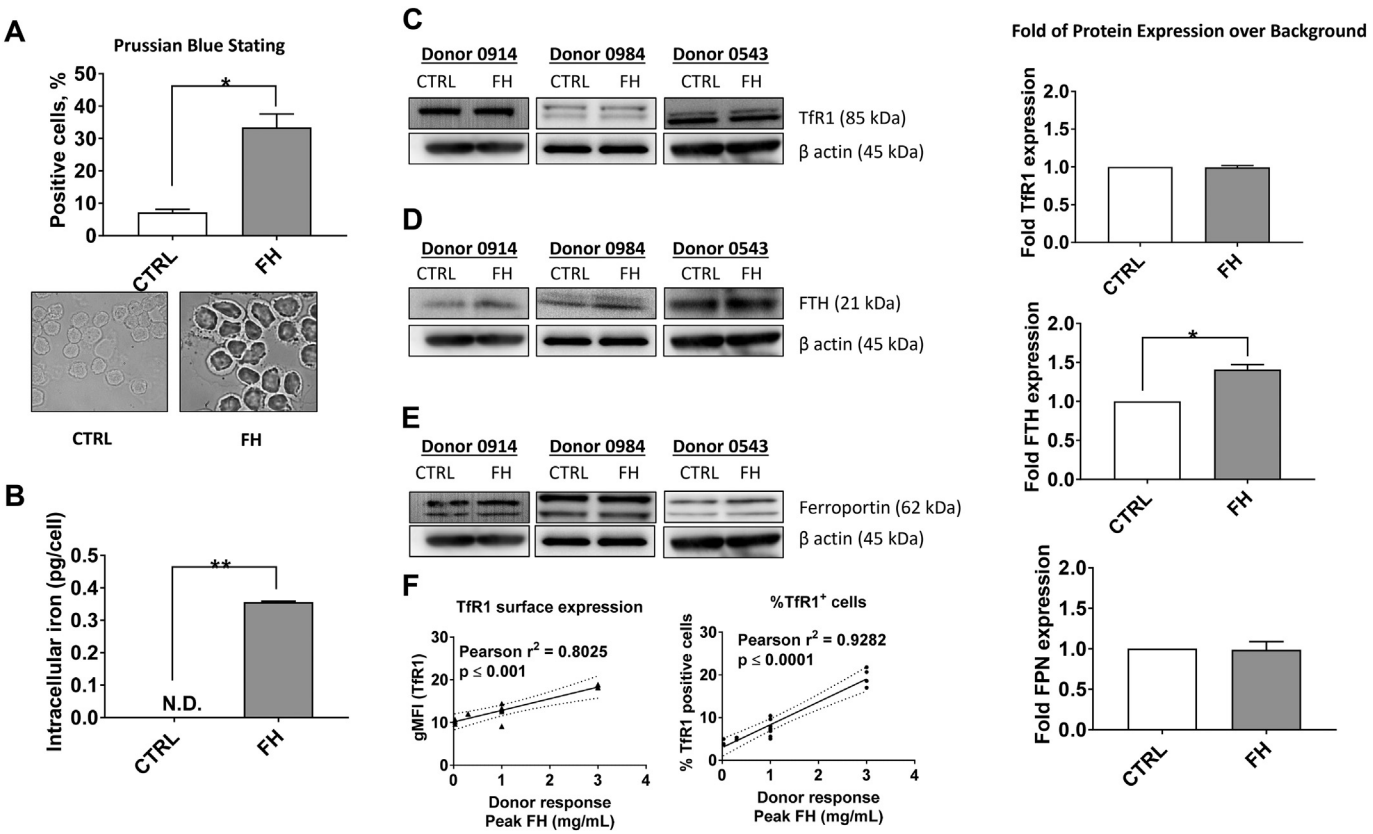

Fig. 4. Feraheme (FH) uptake by primary human T cells. (A) An increase in Prussian blue–positive cells was observed in FH-treated cells compared to the vehicle control. The bar graph below the micrographs shows the percent of positive cells calculated from at least 100 cells in each treatment per donor. The images shown are representative of one donor at 1000 times magnification, and the bar graph is mean ± SEM from 3 donors. (B) Intracellular iron was quantified using ICP-MS, showing an increase in iron concentrations following FH treatment. (C–E) Treatment with FH increased the expression of ferritin, whereas other iron-trafficking proteins remain unchanged. Bar graphs for immunoblots show mean band intensities obtained from 3 donors. (F) The mean fluorescence intensity of baseline TfR1 expression on T cells and the percent of TfR1-positive cells correlated with the donor responsiveness assessed by Δψm. The data are presented in mean ± SEM (n ≥ 3 donors) with experimental duplicates for each donor. * and ** denote p-values of ≤0.05 and ≤ 0.01, respectively. For correlation plots, the Pearson correlation value was determined in 9 different donors from the dose responsiveness pool in Fig. 1B.

Feraheme treatment resulted in an approximately four-fold increase in the number of Prussian blue–positive cells (compare 33.4 ± 4.1% to 7.2 ± 1.0% in the negative control). This finding was further confirmed by the ICP-MS, which detected 0.356 ± 0.003 pg of elemental iron per Feraheme-treated cell (Fig. 4B). The iron levels in the negative control sample were below the instrument's lower limit of detection (Fig. 4B). The levels of iron detected in the Feraheme-treated cells corresponded to approximately 0.1% of the total iron present in the cell culture medium after the Feraheme treatment.

Next, we assessed the levels of proteins involved in iron storage and trafficking. Feraheme treatment increased the levels of ferritin heavy chain (FTH) but not transferrin receptor 1 (TfR1) or ferroportin (FPN) (Fig. 4C–E). Since transferrin-bound iron is internalized via TfR1-mediated endocytosis; we next assessed the levels of TfR1 surface expression using flow cytometry. Although there was no change in the TfR1 expression on T cells after 24 h of treatment with Feraheme (Supplementary Fig. 5), the baseline expression of this receptor varied between individual donors (Fig. 4F). Moreover, the basal TfR1 expression correlated with cellular responsiveness to different concentrations of Feraheme as assessed by measuring for changes in the membrane potential (Fig. 1B).

3.4. Feraheme alters the function of primary human T cells

The changes described above may affect the function of T-cells. To understand such functional effects, we next studied how Feraheme influences the cytokine expression and proliferation of the T cells stimulated with a well-known agonist (PHA/ConA cocktail or CD3-crosslinking antibody). We exposed primary T-cells to Feraheme for 24 h before the stimulation. Untreated cells were used as a control. The cytokine levels were analyzed in the culture supernatants 48 h after the addition of PHA/ConA to both Feraheme-primed and control T-cells. Feraheme-primed cells produced significantly lower levels of cytokines in response to the PHA/ConA treatment than did the control cells (Supplementary Fig. 6 and Fig. 5A). These results were consistent between all tested donors. T-cell proliferation in response to CD3-crosslinking antibody was measured using a BrdU assay 72 h after the agonist addition. Similar to the effects on cytokine secretion, Feraheme treatment reduced proliferation of T cells in response to the CD3 mitogen as compared to the control cells (Fig. 5B). The reduction in T-cell function was not due to the cytotoxicity of Feraheme (Supplementary Fig. 4). Therefore, we hypothesized, that these changes can be reversed by intervening the mitochondrial damage.

3.5. Feraheme-mediated functional changes are reversed by the inhibitor of mitoROS

At the beginning of the study, we found that the generation of mitoROS is one of the mechanisms responsible for the mitochondrial damage. Therefore, we wished to determine if it was also responsible for the alteration in T-cell function which we describe in the previous section of this manuscript. The mitoROS inhibitor MitoTEMPO restored the CD3-induced proliferation index in Feraheme-primed T cells to that seen in the control cells (Fig. 5B). A schematic representation of the

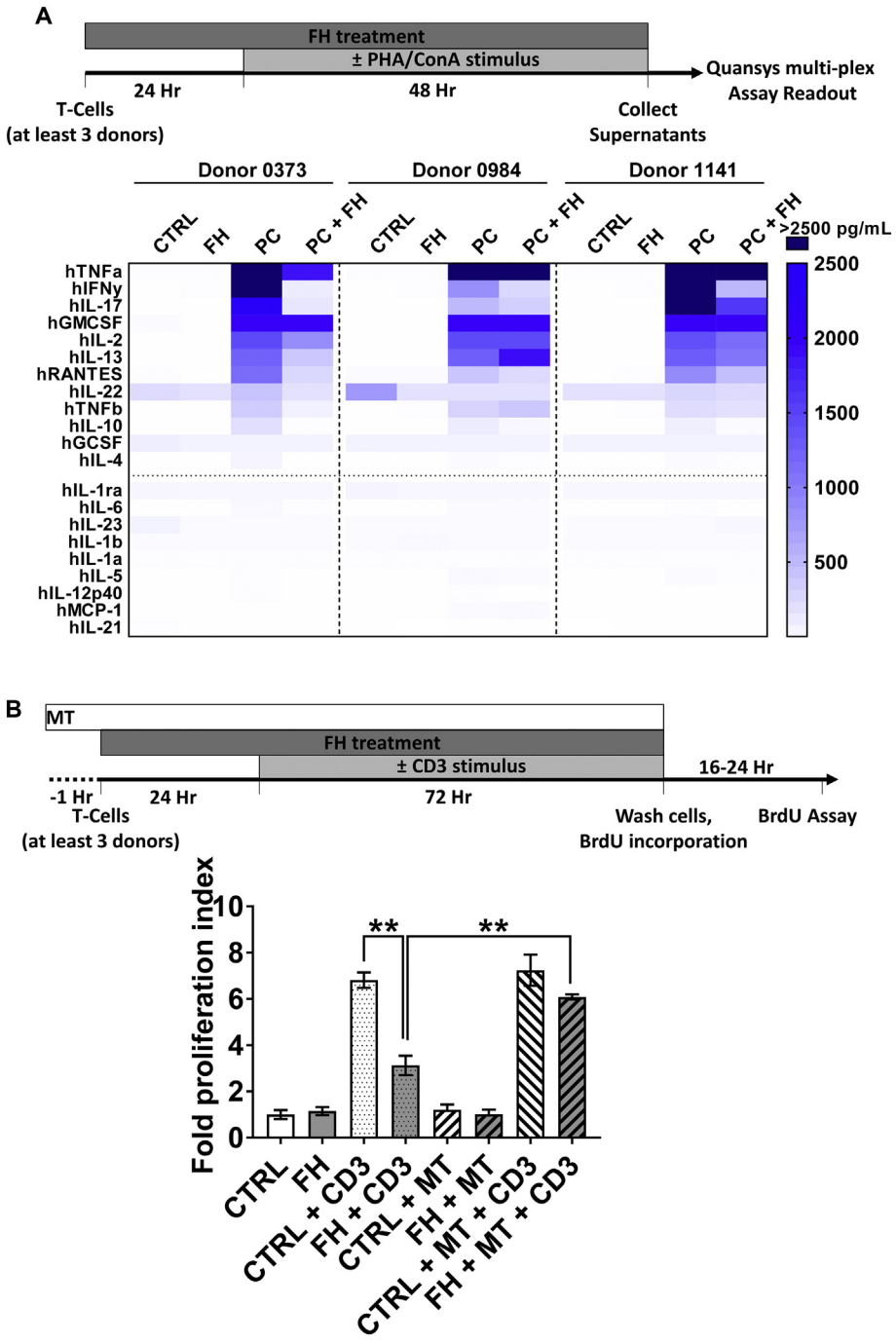

Fig. 5. Feraheme (FH) altered normal primary T-cell function. (A) The treatment protocol for cytokine assessment was followed as shown in this schematic. Each box in the heatmap represents the mean cytokine concentration from experimental replicates. (B) The schematic demonstrates a general experimental timeline for the proliferation assay. FH reduced the CD3-mediated proliferation of primary T cells. Pretreatment with MitoTEMPO (MT) 1 h before the FH treatment restored CD3-mediated T-cell proliferation. The bar graph demonstrates mean ± SEM ($n \geq 4$ donors) with each sample in duplicate for each treatment group. Data were considered statistically significant with a p-value ≤ 0.01 (**).

mechanism leading to the alteration in T-cell function after exposure to Feraheme is shown in Fig. 6.

3.6. *In vitro assay framework is specific to Feraheme and cannot be used for comparison between other IONPs*

The idea of an in vitro experimental framework to enable systematic approach for the preclinical immunotoxicity screening of nanoparticles has been recently proposed elsewhere (Shah and Dobrovolskaia, 2018). Briefly, it relies on the notion that changes in the immune function are difficult to identify in vitro using one assay/one end-point approach and suggests a systematic approach based on a network of in vitro assays (Shah and Dobrovolskaia, 2018). Through the studies described above, we demonstrated that Feraheme is immunosuppressive. According to our data, four in vitro assays (Δψm, mitoROS, cytokine panel, and proliferation index) consistently reveal the Feraheme-mediated immunosuppression in cells from all tested donors, regardless of their individual sensitivity to various concentrations of this formulation. We, therefore, used these assays to compile an in vitro framework (Shah and Dobrovolskaia, 2018) indicative of the Feraheme-mediated immunosuppression. Two assays in this framework, Δψm and mitoROS, are interchangeable because they both assess the mitochondrial changes. We next explored the applicability of the framework to other iron-based complex nanoformulations. We focused on three assays - Δψm, cytokine panel, and proliferation index. The goal of this part of the study was to understand whether the immunosuppressive properties described for Feraheme are unique to this formulation or shared by other iron-based complex nanodrugs.

We compared Feraheme (ferumoxytol-polysorbitol glucose carboxymethyl ether) to Venofer (iron sucrose), Injectafer (ferric

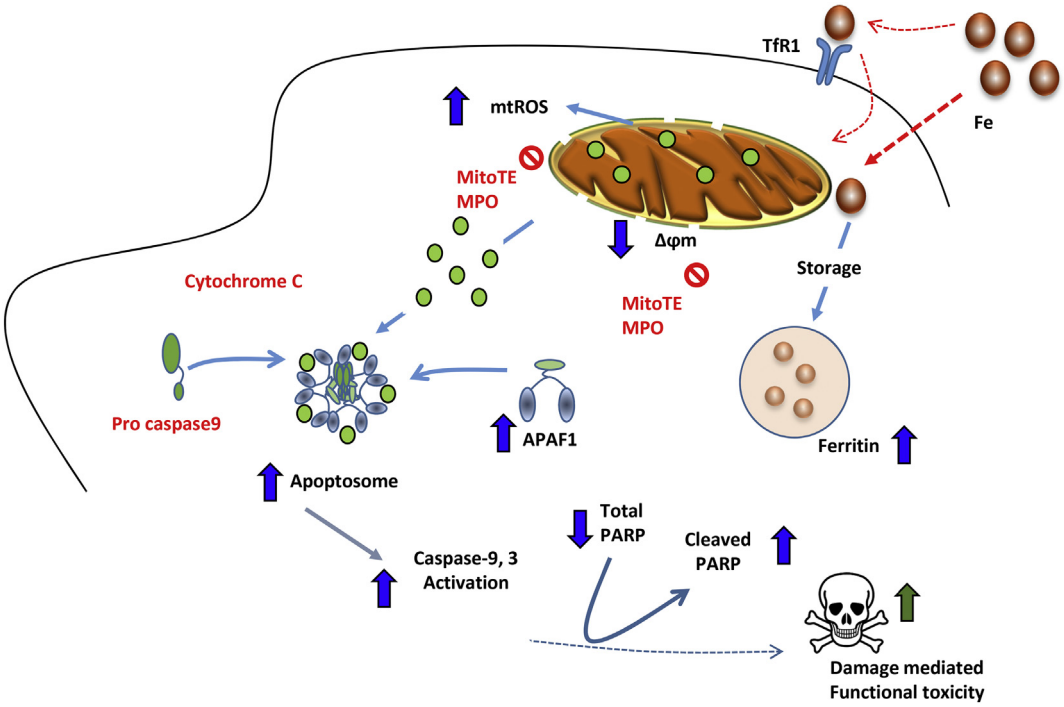

Fig. 6. Schematic representation of the mechanism involved in the Feraheme (FH)-mediated immunosuppression. FH increases intracellular iron concentrations that can increase the iron-storage protein ferritin. Excess intracellular iron then increases mitoROS, which in turn damages mitochondria by altering mitochondrial membrane potential and changing mitochondrial dynamics. The damaged mitochondria then release cytochrome C, which recruits pro-caspase-9 and APAF1. The apoptosome further signals for the activation of caspase-mediated cascades of signals and induces cleavage of PARP. This can eventually lead to functional toxicity in the T cells, which is evidenced by suppression of cytokine and proliferative responses to a known agonist.

carboxymaltose), Ferrlecit (sodium ferric gluconate), and generic sodium ferric gluconate. A comparative physicochemical characterization was performed to assess the hydrodynamic size and zeta potential of these formulations (Table 2 and Supplementary Fig. 7). The ICP-MS was used to quantify the amount of iron (Table 2).

Despite the fact that these formulations were tested at equivalent concentrations of iron, they demonstrated different effects on T cells than those observed with Feraheme. In particular, Venofer, Ferrlecit, and sodium ferric gluconate resulted in a more considerable change in Δψm than Feraheme did, while Injectafer did not affect it at all (Fig. 7A). According to the Prussian blue staining, Venofer and Ferrlecit treatment resulted in a greater accumulation of iron than that observed in the Feraheme-treated cells, while Injectafer-treated cells looked indistinguishable from the negative control (compare Fig. 7B and 4A). Interestingly, the generic-formulation sodium ferric gluconate resulted in lower iron accumulation than its brand counterpart Ferrlecit (Fig. 7B). The findings of the TEM analysis of Venofer- and Ferrlecit-treated cells were in agreement with the Prussian blue staining. Specifically, the cells treated with Venofer and Ferrlecit showed a higher accumulation of particles on the membranes and within the cells (Supplementary Fig. 8, refer to the arrowheads), whereas Injectafer-treated cells looked identical to those in the negative group. Furthermore, the damaged mitochondria, as determined by the remodeling of cristae, were more prominent and deformed in cells treated with Venofer and Ferrlecit, but they were not seen in the Injectafer-treated cells. The general alteration in the mitochondrial dynamics identified in Feraheme-treated cells was also seen in Venofer- and Ferrlecit-treated cells, but not in Injectafer-treated cells. Functional assays revealed that Venofer suppressed mitogen-stimulated cytokines in T cells from all tested donors, similar to that observed in Feraheme-treated cells. Ferrlecit and its generic version, sodium ferric gluconate, had similar effects but were donor-dependent. The Injectafer formulation did not alter mitogen-triggered cytokine release from T cells at all (Fig. 7D). Unlike Feraheme, all iron-based complex formulations increased the CD3 antibody–triggered T-cell proliferation (Fig. 7D).

3.7. Immortalized human T-cell lines do not accurately recapitulate Feraheme's effects on primary T cells

When immunotoxicity studies are conducted during preclinical characterization of nanomaterials in vitro, both primary cells and immortalized cell lines can be used. However, human blood and primary human T cells may not be available to some researchers. At the same time, immortalized cell lines are more broadly accessible. Therefore, we next wanted to verify if some of the well-established T-cell lines can accurately recapitulate the immune responses we observed in the primary T-cell cultures. To do so, we applied the framework to analyze Feraheme's effects on Mo-T, A3, and Loucy cell lines, which have previously been used as representative T-cell lines for in vitro studies (Ben-Bassat et al., 1990; Juo et al., 1998; Kalyanaraman et al., 1982). The results of our study demonstrate that none of these cell lines accurately recapitulate the Feraheme effects observed in the human primary T cells (Table 1).

4. Discussion

In this study, we explored the idea of streamlining current approaches for the immunotoxicity assessment of IONPs by compiling an in vitro assay framework that would allow for the detection of intracellular and functional changes in the IONP-exposed cells. To explore the idea, we chose one clinically relevant IONP formulation, Feraheme, with known immunomodulatory properties. An analysis of available literature data and our experience with this formulation in the Nanotechnology Characterization Laboratory preclinical assay cascade suggested that Feraheme exhibits its immunomodulation through the effects on T cells. We verified this hypothesis by analyzing the effects of Feraheme on the primary human T cells in vitro.

Feraheme treatment led to the changes in mitochondrial membrane

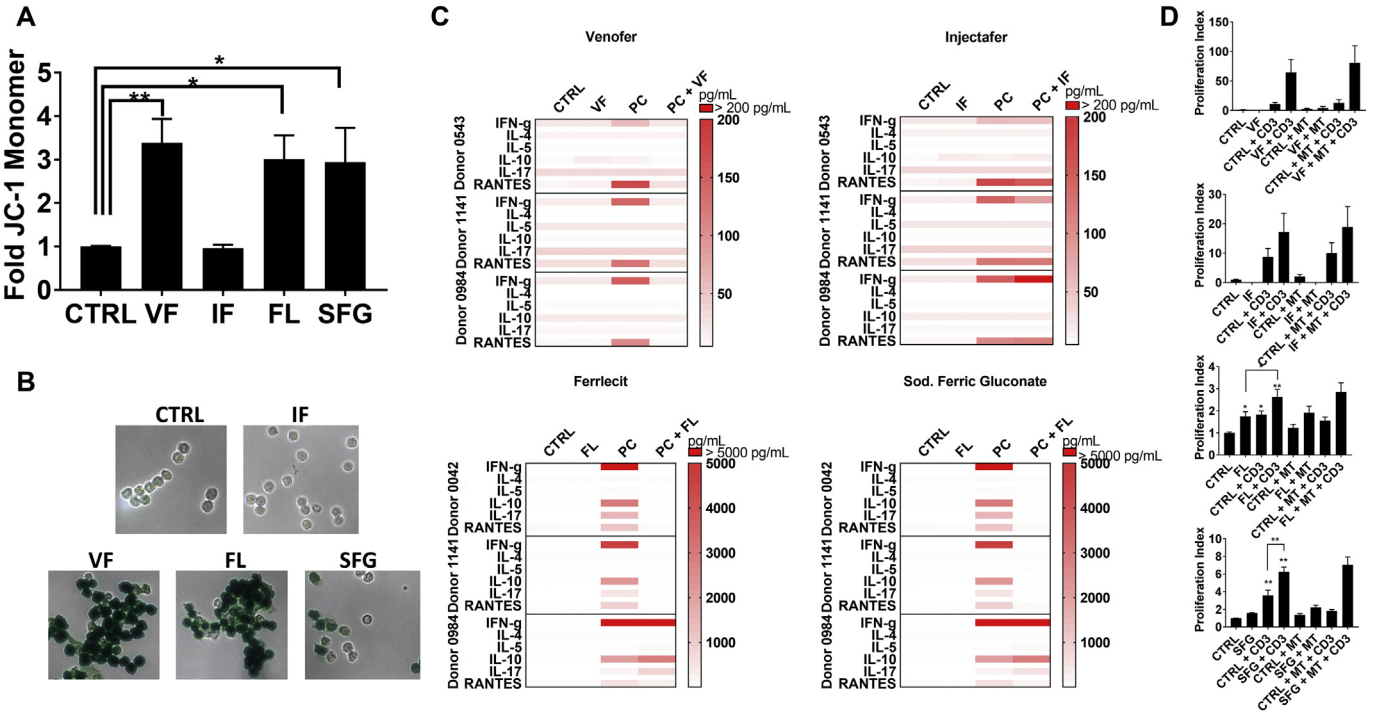

Fig. 7. Framework compiled using Feraheme (FH) as a model particle does not apply to other iron-based complex drug formulations. The applicability of the framework developed with FH was assessed for Venofer (VF), Injectafer (IF), Ferrlecit (FL), and sodium ferric gluconate (SFG) at the optimal concentrations for respective donors. (A) Assessment of mitochondrial membrane potential using a JC-1 assay showed a higher Δψm with VF, FL, and SFG (B) Treatment with VF, FL, and SFG showed Prussian blue–positive T cells, whereas IF-treated cells were unchanged compared to those in the control. (C) VF, FL, and SFG reduced cytokine expressions observed with mitogen-activated T cells, whereas IF-treated cells did not alter mitogen-induced cytokine expressions. (D) All of the iron-based complex drug formulations increased mitogen-activated T-cell proliferation, which remained unchanged despite pretreatment with MitoTEMPO. The bar graphs demonstrate mean ± SEM (n ≥ 3 donors) with each sample in duplicate for each treatment group. Data were considered statistically significant with a p-value ≤0.05 (*) or 0.01 (**).

Table 1
Responsiveness of immortalized T-cell lines to Feraheme in vitro. The framework established in PBMC was applied to cell lines. While Feraheme tested positive in all assays when analyzed in PBMC, individual T-cell lines were unable to recapitulate these responses.

Cell-Line	Δψm assay	mitoROS assay	Cytokines	Proliferation assay
A3	–	–	–	–
Mo-T	–	+	+	–
Loucy	+	–	+	–

potential (Fig. 1A and C) and induced the generation of mitoROS (Fig. 1D, E). Unlike previous reports demonstrating an induction of total ROS by IONPs in monocytes and macrophages (Park et al., 2014; Zhu et al., 2011), we did not observe total oxidative stress in T cells (Fig. 1F). It has been reported that mitochondria can produce ROS during an electron transfer chain that utilizes iron (Lenaz, 1998; Cecchini, 2003; Lill et al., 2012). Therefore, we hypothesize that dysregulation of intracellular iron levels can disrupt mitochondrial redox and exacerbate the damage. In support of this hypothesis are our data that demonstrate the change in mitochondrial dynamics (Fig. 2) and iron accumulation in the cells after Feraheme treatment (Fig. 4A and B). The data also suggest that the generation of mitoROS by T cells in response to Feraheme is insufficient to induce total redox imbalance at the cellular level and is restricted to the organelle level.

Mitochondrial damage is implicated in a wide range of toxicities, including those contributing to neurological disorders (Bennett and Griffiths, 2013), cardiotoxicity (Penna et al., 2013), and immune dysfunction (Kepp et al., 2014). Moreover, apoptotic cascades and anti-apoptotic signaling molecules are tightly regulated by healthy mitochondria. ROS, mitochondrial damage and apoptosis are tightly interrelated. Therefore, we hypothesized that activation of pro-apoptotic signaling should accompany Feraheme effects on T-cells. We used qualitative approach to probe the levels of individual proteins involved in the pro-apoptotic signaling. The results of these tests suggest that activation of the pro-apoptotic signaling cascade indeed takes place (Fig. 3). Interestingly, this activation was not associated with the cell death (Supplementary Fig. 4). It is likely, that the markers of pro-apoptotic cascade activation are very sensitive to mitochondrial perturbation, and allow detection of the cell damage before more dramatic impact on the cell viability become evident. Nevertheless, despite the lack of cytotoxicity, the observed changes in the mitochondria (Fig. 1) and activation of the pro-apoptotic signaling (Fig. 3), collectively contribute to the perturbation of the T-cell function, as evidenced by the inhibition of the cytokine and proliferative response to known T-cell agonists (Fig. 5).

We confirmed this hypothesis in several experiments. First, we demonstrated that mitochondrial damage and mitoROS generation could be inhibited by the addition of a mitochondria-specific antioxidant, MitoTEMPO (Fig. 1D and F). Next, we showed that the addition of MitoTEMPO reverts Feraheme-mediated immunosuppression and restores T cells' proliferative responses to a known mitogen (Fig. 5B). Collectively, the results demonstrating mitochondrial damage, generation of mitoROS, change in mitochondrial dynamics, and subsequent changes in the T-cell function (Figs. 1–3, and Fig. 5) suggest that an alteration in mitochondrial dynamics due to Feraheme treatment is a reflection of cellular stress. These data are also consistent with the literature reports demonstrating that both mitofusion and mitofission are implicated in the cellular response to stress (Youle and van der Bliek, 2012). The data demonstrating that Feraheme suppresses the secretion of RANTES, IFNγ, IL-4, IL-5, IL-10, and IL-17 in the mitogen-activated T cells (Fig. 5A) agree with the previous reports demonstrating a

Table 2
Physicochemical characterization of nanoparticles analyzed in this study. The table summarizes the information provided in the product inserts of individual iron-based nanomaterials with regards to composition, coating and the concentration of iron as reported by the manufacturers. The table further includes nanoparticle hydrodynamic size measured by DLS, zeta potential, and iron concentration measured by ICP-MS as described in the materials and methods.

Formulation	Brand/ generic	Nominal iron core size (nm)	Chemical formula	Coating material	Size by DLS, nm	Zeta potential (mV)	Reported iron concentrations (mg/mL)	Measured iron concentrations (mg/mL)
Feraheme	Brand	17–31	Non-stoichiometric Fe_2O_3 ($Fe_{5874}O_{8752}$·$C_{11719}H_{18682}O_{9933}Na_{414}$)	Polyglucose sorbitol carboxy-methylether	32.4 (1.2)	−0.362 (0.478)	30	28.8 ± 0.7
Venofer	Brand	NR	Polynuclear Iron (III) hydroxide $(Na_2Fe_5O_8(OH)\cdot 3(H_2O))_n \cdot m(C_{12}H_{22}O_{11})$	Sucrose	12.7 (0.3)	−1.19 (0.25)	20	19.3 ± 0.3
Injectafer	Brand	NR	Polynuclear Iron (III) hydroxide $(FeO_x(OH)_y(H_2O)_z]_n$ $[\{(C_6H_{10}O_5)_m\ (C_6H_{12}O_7)\}_l]_k$, n ≈ 103, m ≈ 8, l ≈ 11, and k ≈ 4)	Dextran	28.4 (0.5)	−1.75 (0.89)	50	48.9 ± 1.6
Ferrlecit	Brand	NR	Macromolecular complex of ferric oxide $([NaFe_2O_3(C_6H_{11}O_7)\ (C_{12}H_{22}O_{11})_5]\ n \approx 200^*)$	Sodium gluconate complex	19.9 (1.1)	−0.1 (0.8)	12.5	12.6 ± 0.2
Sodium ferric gluconate	Generic	NR	Macromolecular complex of ferric oxide $([NaFe_2O_3(C_6H_{11}O_7)\ (C_{12}H_{22}O_{11})_5]\ n \approx 200^*)$	Sodium gluconate complex	12.8 (3.2)	−2.90 (1.08)	12.5	13.1 ± 0.4

NR: not reported.

suppression of PHA/ConA- or OVA-mediated cytokines by dextran-coated IONPs in rat lymphocytes (Easo and Mohanan, 2015). The immunosuppression may have both negative and positive consequences to the host. Undesirable immunosuppression is a safety concern because it lowers the host's resistance to pathogens and cancer (Ghirelli and Hagemann, 2013; George et al., 2014). However, under certain conditions, such as autoimmunity, suppression of the T cell–mediated responses is beneficial. We, therefore, suggest that Feraheme-mediated immunosuppression may have beneficial effects in patients with autoimmune disorders. A retrospective analysis of patients receiving Feraheme for iron deficiency indication might be helpful in verifying our hypothesis. However, the clinical data regarding autoimmune disorders in iron-deficient patients are not available.

Since both Prussian blue staining (Fig. 4A) and ICP-MS (Fig. 4B) confirmed an increase in the intracellular iron following Feraheme treatment, we next assessed the expression of proteins known to play critical roles in iron import, storage, and export. These proteins are TfR1, TFH, and FPN. We tested the expression of TfR1 on T cells before and after exposure to Feraheme. Interestingly, the TfR1 receptor expression on the resting T cells correlated with their responsiveness to various concentrations of Feraheme (Fig. 4F). Previously, soluble TfR1 in the serum has been proposed to be a valuable prognostic biomarker for various conditions, including iron deficiency (Beguin, 2003; Li et al., 2008; Rosager et al., 2017). Our findings of TfR1 expression on the surface of resting T cells suggest that it could provide predictive estimates of a donor's responsiveness to Feraheme during in vitro immunotoxicity assessment. However, the predictive value of TfR1 expression in immunosuppressive responses of individual patients in vivo has yet to be confirmed. The expression of TfR1 did not change after the treatment with Feraheme, nor did the expression of the FPN (Fig. 4C). However, the levels of FTH increased (Fig. 4D). These data demonstrate that T cells responded to the increased intracellular iron levels and associated with its stress by upregulating their iron-storage machinery. Neither the iron import mechanisms nor export mechanisms were altered (Fig. 4C–E). Our in vitro finding is consistent with the clinical data demonstrating that Feraheme treatment increases the serum ferritin levels (Lu et al., 2010; FERAHEME® (ferumoxytol) Injection [package insert], AMAG Pharmaceuticals, 2015).

Despite the successful demonstration of Feraheme-mediated intracellular iron increase by multiple methods, our ability to identify the precise mechanism triggering this increase is limited by the sensitivity of the available methodology. Specifically, we cannot discriminate whether Feraheme releases iron ions in the culture medium or is taken up by the T cells in a nanoparticulate form and then releases the iron ions inside the cell. Traditionally, TEM is the method of choice for the detection of particle uptake by cells, and the available literature has been successful in identifying intracellular IONPs in phagocytic cells, such as monocytes and macrophages, which engulf large quantities of particles (Chen et al., 2011; Grosse et al., 2016). T cells, however, are not phagocytic. Therefore, a priori, one would not expect a massive uptake of the particulates by these cells. Our TEM images (Fig. 2) do not reveal any signs of the particulates' presence in the Feraheme-treated T cells. However, we cannot conclude that Feraheme is not internalized by the cells in particulate form because we know from the ICP-MS study (Fig. 4B) that the amount of iron per individual cell is approximately 0.3 pg/cell, which is lower than the TEM sensitivity. Therefore, the important question of whether the Feraheme is taken up by the T cells in a nanoparticulate form has yet to be answered. To explore the potential involvement of various endocytic routes, we performed experiments with specific inhibitors for micropinocytosis-, scavenger-receptor-, clathrin- and caveolin-mediated endocytosis. None of these inhibitors affected Feraheme-triggered $\Delta\psi m$ (data not shown), suggesting that these pathways may not be involved in Feraheme-mediated mitochondrial damage to the extent that would be detectable in vitro.

Prior studies have reported that the expression of CD25 and CD69 may serve as functional markers for T-cell activation. When we assessed

the expression of these markers in vitro in the Feraheme-treated cells, the responses were inconsistent between donors and not robust (data not shown), and we, therefore, excluded these markers from further consideration. Instead, we chose several assays that demonstrated consistent results among the donors and included both the mechanistic (JC-1 monomer formation and mitoROS generation) and functional (effects on mitogen-mediated proliferation and cytokine secretion) endpoints, which also showed a cause-effect relationship. These assays comprise a framework that we propose for comparison between Feraheme and its generic versions. Since no generic ferumoxytol-polysorbitol glucose carboxymethyl ether is currently available, we could not verify the performance of this formulation in the proposed framework. Next, we wanted to understand if this framework is specific to Feraheme or if it can also be applied to the broad class of other clinically relevant iron-based complex formulations (Table 1). The results of our investigation (Fig. 7) suggest that the difference in the coating material, chemical and molecular properties, particle size, and availability of iron can affect the performance and applicability of the framework. Earlier studies have demonstrated that the labile iron concentrations in these formulations are different (Jahn et al., 2011), which can contribute to the difference in their clinical efficacy. It is very likely that the immunotoxicity associated with these formulations could also depend on the labile iron. It is plausible to assume that the framework established using Feraheme is strictly applicable for its generic formulations. Additional studies are needed to get a better insight into the differential responses observed with a broad range of iron-oxide complex formulations. Similarly, a complete understanding of the various physicochemical properties of Feraheme would require a systematic structure-activity relationship study in which the same coating material is used with an iron core of different sizes. Certain logistical challenges associated with the availability of the coating and the synthetic procedure needed to attach it to iron cores with varying size precluded us from conducting such analysis in this study. Another significant finding of our study is that immortalized T-cell lines do not recapitulate Feraheme's effects on primary human T cells. Therefore, the framework intended to identify similarity of generic formulations to Feraheme should utilize T lymphocytes freshly isolated from human blood.

In conclusion, the results of our study extend current understanding of the Feraheme safety profile by supplementing existing literature regarding the acute immunotoxicity (i.e., complement-mediated pseudoallergy and immediate type hypersensitivity reactions) with the mechanistic understanding of the long-term immunotoxicity (i.e., inhibition of the T-cell function). The mechanistic framework described in this study can be used to compare Feraheme with its generic versions and serve as a strategic baseline for the immunotoxicity evaluation of other iron-oxide formulations.

Acknowledgments

The study was supported in whole or in part by federal funds from the National Cancer Institute, National Institutes of Health, under contract HHSN261200800001E. The content of this publication does not necessarily reflect the views or policies of the Department of Health and Human Services, nor does mention of trade names, commercial products, or organizations imply endorsement by the U.S. Government. M.A.D. is grateful to Dr. Scott E. McNeil for continuous support.

Authors contributions

A.S. carried out all immunological experiments. C.I.M performed ICP-MS and TEM analysis of nanoparticle samples. A.V. performed DLS analysis. J.C. supervised the analysis performed by C.I.M and A.V. and analyzed DLS, ICP-MS and TEM data. F.S. performed TEM analysis of the cells treated with nanoparticles. M.A.D. conceived, designed, and supervised this study. A.S. and M.A.D. analyzed and interpreted all data, and wrote the manuscript. All authors contributed to the manuscript preparation.

Appendix A. Supplementary data

Supplementary data to this article can be found online at https://doi.org/10.1016/j.taap.2018.04.028.

References

Beguin, Y., 2003. Soluble transferrin receptor for the evaluation of erythropoiesis and iron status. Clin. Chim. Acta 329 (1–2), 9–22.
Ben-Bassat, H., Shlomai, Z., Kohn, G., Prokocimer, M., 1990. Establishment of a human T-acute lymphoblastic leukemia cell line with a (16;20) chromosome translocation. Cancer Genet. Cytogenet. 49 (2), 241–248.
Bennett, S.J., Griffiths, H.R., 2013. Regulation of T-Cell Functions by Oxidative Stress. In: Alcaraz, M.J., Gualillo, O., Sánchez-Pernaute, O. (Eds.), Studies on Arthritis and Joint Disorders. Springer New York, New York, NY, pp. 33–48.
Cecchini, G., 2003. Function and structure of complex II of the respiratory chain. Annu. Rev. Biochem. 72, 77–109.
Chen, C.L., Zhang, H., Ye, Q., Hsieh, W.Y., Hitchens, T.K., Shen, H.H., et al., 2011. A new nano-sized iron oxide particle with high sensitivity for cellular magnetic resonance imaging. Mol. Imaging Biol. 13 (5), 825–839.
Di Gioacchino, M., Petrarca, C., Lazzarin, F., Di Giampaolo, L., Sabbioni, E., Boscolo, P., et al., 2011. Immunotoxicity of nanoparticles. Int. J. Immunopathol. Pharmacol. 24 (1 Suppl), 65S–71S.
Easo, S.L., Mohanan, P.V., 2015. In vitro hematological and in vivo immunotoxicity assessment of dextran stabilized iron oxide nanoparticles. Colloids Surf B Biointerfaces 134, 122–130.
Eleftheriadis, T., Pissas, G., Liakopoulos, V., Stefanidis, I., 2016. Cytochrome *c* as a potentially clinical useful marker of mitochondrial and cellular damage. Front. Immunol. 7, 279.
FERAHEME® (ferumoxytol) Injection [package insert], AMAG Pharmaceuticals, Inc. Waltham, MA. 2015.
Gaharwar, U.S., Meena, R., Rajamani, P., 2017 Oct. Iron oxide nanoparticles induced cytotoxicity, oxidative stress and DNA damage in lymphocytes. J. Appl. Toxicol. 37 (10), 1232–1244. http://dx.doi.org/10.1002/jat.3485.
George, M.P., Masur, H., Norris, K.A., Palmer, S.M., Clancy, C.J., McDyer, J.F., 2014. Infections in the immunosuppressed host. Ann Am Thorac Soc. 11 (Suppl. 4), S211–20.
Ghirelli, C., Hagemann, T., 2013. Targeting immunosuppression for cancer therapy. J. Clin. Invest. 123 (6), 2355–2357.
Grosse, S., Stenvik, J., Nilsen, A.M., 2016. Iron oxide nanoparticles modulate lipopolysaccharide-induced inflammatory responses in primary human monocytes. Int. J. Nanomedicine 11, 4625–4642.
Hempel, J.C., Poppelaars, F., Gaya da Costa, M., Franssen, C.F.M., de Vlaam, T.P.G., Daha, M.R., et al., 2017. Distinct in vitro complement activation by various intravenous iron preparations. Am. J. Nephrol. 45 (1), 49–59.
Jahn, M.R., Andreasen, H.B., Futterer, S., Nawroth, T., Schunemann, V., Kolb, U., et al., 2011. A comparative study of the physicochemical properties of iron isomaltoside 1000 (Monofer), a new intravenous iron preparation and its clinical implications. Eur. J. Pharm. Biopharm. 78 (3), 480–491.
Juo, P., Kuo, C.J., Yuan, J., Blenis, J., 1998. Essential requirement for caspase-8/FLICE in the initiation of the Fas-induced apoptotic cascade. Curr. Biol. 8 (18), 1001–1008.
Kalyanaraman, V.S., Sarngadharan, M.G., Robert-Guroff, M., Miyoshi, I., Golde, D., Gallo, R.C., 1982. A new subtype of human T-cell leukemia virus (HTLV-II) associated with a T-cell variant of hairy cell leukemia. Science 218 (4572), 571–573.
Kepp, O., Senovilla, L., Vitale, I., Vacchelli, E., Adjemian, S., Agostinis, P., et al., 2014. Consensus guidelines for the detection of immunogenic cell death. Oncoimmunology 3 (9), e955691.
Kroemer, G., Galluzzi, L., Brenner, C., 2007. Mitochondrial membrane permeabilization in cell death. Physiol. Rev. 87 (1), 99–163.
Lenaz, G., 1998. Role of mitochondria in oxidative stress and ageing. Biochim. Biophys. Acta 1366 (1–2), 53–67.
Li, Y.Q., Yan, H., Bai, B., 2008. Change in iron transporter expression in human term placenta with different maternal iron status. Eur. J. Obstet. Gynecol. Reprod. Biol. 140 (1), 48–54.
Li, K., Nejadnik, H., Daldrup-Link, H.E., 2017. Next-generation superparamagnetic iron oxide nanoparticles for cancer theranostics. Drug Discov. Today 22 (9), 1421–1429.
Lill, R., Hoffmann, B., Molik, S., Pierik, A.J., Rietzschel, N., Stehling, O., et al., 2012. The role of mitochondria in cellular iron-sulfur protein biogenesis and iron metabolism. Biochim. Biophys. Acta 1823 (9), 1491–1508.
Lu, M., Cohen, M.H., Rieves, D., Pazdur, R., 2010. FDA report: Ferumoxytol for intravenous iron therapy in adult patients with chronic kidney disease. Am. J. Hematol. 85 (5), 315–319.
Lunov, O., Syrovets, T., Buchele, B., Jiang, X., Rocker, C., Tron, K., et al., 2010. The effect of carboxydextran-coated superparamagnetic iron oxide nanoparticles on c-Jun N-terminal kinase-mediated apoptosis in human macrophages. Biomaterials 31 (19), 5063–5071.
Naqvi, S., Samim, M., Abdin, M., Ahmed, F.J., Maitra, A., Prashant, C., et al., 2010. Concentration-dependent toxicity of iron oxide nanoparticles mediated by increased oxidative stress. Int. J. Nanomedicine 5, 983–989.
Nedyalkova, M., Donkova, B., Romanova, J., Tzvetkov, G., Madurga, S., Simeonov, V.,

2017 Nov. Iron oxide nanoparticles - in vivo/in vitro biomedical applications and in silico studies. Adv. Colloid Interface Sci. 249, 192–212. http://dx.doi.org/10.1016/j.cis.2017.05.003.
Ow, Y.P., Green, D.R., Hao, Z., Mak, T.W., 2008. Cytochrome c: functions beyond respiration. Nat. Rev. Mol. Cell Biol. 9 (7), 532–542.
Pai, A.B., Conner, T., McQuade, C.R., Olp, J., Hicks, P., 2011. Non-transferrin bound iron, cytokine activation and intracellular reactive oxygen species generation in hemodialysis patients receiving intravenous iron dextran or iron sucrose. Biometals 24 (4), 603–613.
Park, E.J., Choi, D.H., Kim, Y., Lee, E.W., Song, J., Cho, M.H., et al., 2014. Magnetic iron oxide nanoparticles induce autophagy preceding apoptosis through mitochondrial damage and ER stress in RAW264.7 cells. Toxicol. in Vitro 28 (8), 1402–1412.
Park, E.J., Oh, S.Y., Lee, S.J., Lee, K., Kim, Y., Lee, B.S., et al., 2015. Chronic pulmonary accumulation of iron oxide nanoparticles induced Th1-type immune response stimulating the function of antigen-presenting cells. Environ. Res. 143 (Pt A), 138–147.
Penna, C., Perrelli, M.G., Pagliaro, P., 2013. Mitochondrial pathways, permeability transition pore, and redox signaling in cardioprotection: therapeutic implications. Antioxid. Redox Signal. 18 (5), 556–599.
Perelman, A., Wachtel, C., Cohen, M., Haupt, S., Shapiro, H., Tzur, A., 2012. JC-1: alternative excitation wavelengths facilitate mitochondrial membrane potential cytometry. Cell Death Dis. 3, e430.
Pouliquen, D., Le Jeune, J.J., Perdrisot, R., Ermias, A., Jallet, P., 1991. Iron oxide nanoparticles for use as an MRI contrast agent: pharmacokinetics and metabolism. Magn. Reson. Imaging 9 (3), 275–283.
Rosager, A.M., Sorensen, M.D., Dahlrot, R.H., Hansen, S., Schonberg, D.L., Rich, J.N., et al., 2017. Transferrin receptor-1 and ferritin heavy and light chains in astrocytic brain tumors: expression and prognostic value. PLoS One 12 (8), e0182954.
Sabareeswaran, A., Ansar, E.B., Harikrishna Varma, P.R., Mohanan, P.V., Kumary, T.V., 2016. Effect of surface-modified superparamagnetic iron oxide nanoparticles (SPIONS) on mast cell infiltration: an acute in vivo study. Nanomedicine 12 (6), 1523–1533.
Sadauskas, E., Danscher, G., Stoltenberg, M., Vogel, U., Larsen, A., Wallin, H., 2009. Protracted elimination of gold nanoparticles from mouse liver. Nanomedicine 5 (2), 162–169.
Shah, A., Dobrovolskaia, M.A., 2018. Immunological effects of iron oxide nanoparticles and iron-based complex drug formulations: therapeutic benefits, toxicity, mechanistic insights, and translational considerations. Nanomedicine 14 (3), 977–990.
Shen, C.C., Wang, C.C., Liao, M.H., Jan, T.R., 2011a. A single exposure to iron oxide nanoparticles attenuates antigen-specific antibody production and T-cell reactivity in ovalbumin-sensitized BALB/c mice. Int. J. Nanomedicine 6, 1229–1235.
Shen, C.C., Liang, H.J., Wang, C.C., Liao, M.H., Jan, T.R., 2011b. A role of cellular glutathione in the differential effects of iron oxide nanoparticles on antigen-specific T cell cytokine expression. Int. J. Nanomedicine 6, 2791–2798.
Shen, C.C., Liang, H.J., Wang, C.C., Liao, M.H., Jan, T.R., 2012. Iron oxide nanoparticles suppressed T helper 1 cell-mediated immunity in a murine model of delayed-type hypersensitivity. Int. J. Nanomedicine 7, 2729–2737.
Turcheniuk, K., Tarasevych, A.V., Kukhar, V.P., Boukherroub, R., Szunerits, S., 2013. Recent advances in surface chemistry strategies for the fabrication of functional iron oxide based magnetic nanoparticles. Nano 5 (22), 10729–10752.
Umbreit, T.H., Francke-Carroll, S., Weaver, J.L., Miller, T.J., Goering, P.L., Sadrieh, N., et al., 2012. Tissue distribution and histopathological effects of titanium dioxide nanoparticles after intravenous or subcutaneous injection in mice. J. Appl. Toxicol. 32 (5), 350–357.
Valdiglesias, V., Fernandez-Bertolez, N., Kilic, G., Costa, C., Costa, S., Fraga, S., et al., 2016. Are iron oxide nanoparticles safe? Current knowledge and future perspectives. J. Trace Elem. Med. Biol. 38, 53–63.
Wysowski, D.K., Swartz, L., Vicky Borders-Hemphill, B., Goulding, M.R., Dormitzer, C., 2010. Use of parenteral iron products and serious anaphylactic-type reactions. Am. J. Hematol. 85 (9), 650–654.
Yan, L., Liu, X., Liu, W.X., Tan, X.Q., Xiong, F., Gu, N., et al., 2015. Fe2O3 nanoparticles suppress Kv1.3 channels via affecting the redox activity of Kvbeta2 subunit in Jurkat T cells. Nanotechnology 26 (50), 505103.
Youle, R.J., van der Bliek, A.M., 2012. Mitochondrial fission, fusion, and stress. Science 337 (6098), 1062–1065.
Zhu, M.T., Wang, B., Wang, Y., Yuan, L., Wang, H.J., Wang, M., et al., 2011. Endothelial dysfunction and inflammation induced by iron oxide nanoparticle exposure: risk factors for early atherosclerosis. Toxicol. Lett. 203 (2), 162–171.